Chapter 2

Raman Investigations of Atomic/Molecular Clusters and Aggregates

Zhixun Luo and Jiannian Yao

Additional information is available at the end of the chapter

http://dx.doi.org/10.5772/66098

Abstract

Efforts to tune optic responses of molecular aggregates often alter the characteristics and performance of functional materials, revealing that chemical properties largely rely on molecular stacking and interactions. Although the intrinsic nature of materials is primarily determined by single-molecule structures, molecular aggregation behavior that determines material property resembles the architectural style of a building in which the bricks themselves could be less important. While the establishment of surface-enhanced Raman spectroscopy (SERS) inspired numerous research interest for trace analysis up to single-molecule level, Raman spectroscopy is also recognized for its importance in solving several issues relating to molecule aggregates owing to the capability of non-destructive detection and spectral fingerprints by which chemical structures and aggregation states can be identified. Raman spectroscopy is not only applied to identify chemicals at the gas phase, liquid phase and solid state and to monitor in-situ reactions of materials at reduced sizes but also to probe gas-to-particle conversion in aerosols, microcrystal magnetization and phase transition at aggregated states, which are believed to attract uprising research interest in the near future.

Keywords: molecular aggregates, clusters, Raman spectroscopy, SERS, aggregation-induced resonance

1. Introduction

Aggregation structures such as those of hydrophobic and hydrophilic surfactant molecules widely exist in aqueous solutions, micelles, liquid crystals, various membranes, and biological systems and are important for understanding physical and chemical properties and functions. Extensive investigations have demonstrated that optic responses of molecular aggregates

often determine the property and performance of optical functional materials [1–3]. Also found was that, selective controlling of excitonic states of molecular aggregates profits to engineer optical properties of promising photonic materials described in terms of the model of Frenkel excitons [4–6]. In poor solvents, self-assembly of organic molecules in the form of weakly coupled aggregates display significantly different spectroscopic behavior compared to their monomers [7]. From UV-vis spectral analysis based on Kasha exciton theory [8–10], typical aggregation behavior can be determined by checking out a tilt angle of molecular stacking [11–13]. In addition to UV-vis absorption, fluorescence of aggregates has also been meticulously investigated, where the fluorescence intensity of organic molecules often diminishes upon aggregation due to intermolecular interactions [14–18], but allowing for interesting exceptions such as those demonstrated as aggregation-induced emission enhancement (AIEE), revealing relationships between molecular structures/molecular arrangements and emission properties [2, 3, 19–21]. While numerous UV-vis and fluorescence investigations help determine the aggregation behavior, it is important to utilize vibrational spectroscopic fingerprints of molecular aggregates to identify the components and structures, phase transition, likely isomers, and conformation transition of chemicals at reduced sizes [22, 23].

Raman effect arises when light impinges upon a molecule or molecule aggregates and interacts with the electron cloud and chemical bonds. A fascinating world of Raman spectroscopy toward both bulk materials and single molecules has been fully demonstrated (i.e., the two ends), but for molecule aggregates, there are relatively less Raman spectroscopic studies in reported publications so far. A few Raman investigations have shed light on ionic surfactants [24–28] and photogenerating reactions [29–31] of organic molecule assemblies; and in-situ Raman techniques have been utilized to monitor real-time reactions and catalysis [32–36], as well as photo-induced polymerization and magnetization [37]. Recently, it was reported that small organic molecules could form uniform assembly with head-to-tail J-aggregation along the inner walls of the pores of an anodic aluminum oxide (AAO) template, giving rise to an interesting topic for surface-enhanced Raman spectroscopy [11, 13, 38]. Also, there were a few surface-enhanced Raman spectroscopy (SERS) investigations endeavoring to determine the plasmonic property of metal clusters and structural information of molecule aggregates. Raman spectroscopic studies of atomic/molecular clusters and aggregates are expected to become a significant solution to identify chemical structures at primary state of nucleation and growth of materials, gas-to-particle conversion mechanism of aerosols, as well as the aggregation states in liquid crystals, micelles, bilayers/monolayers, and biomembranes. These efforts also help understand the fundamentals in various fields such as catalysis, optics, magnetism, and medicine, etc.

2. Raman theory of aggregated molecules

According to the molecular exciton theory developed by Davydov [9] and Kasha [8, 10], the aggregation of molecules alters their absorption spectrum, reflecting hypsochromic (i.e., blue-shift) or bathochromic (i.e., red shift) absorption bands, corresponding to H-aggregate (face-to-face, or side-by-side) or J-aggregate (head-to-tail, or linear herring bone) absorptions,

http://dx.doi.org/10.5772/66098

respectively. Assuming that different accumulations of molecules have different tilt angles (defined as the angle between the transition dipole and the molecular axis of the aggregate), typical H-aggregates bear a tilt angle value greater than 54.7° and exhibit a broader, blue-shifted absorption band, while J-aggregates bear a tilt angle smaller than 54.7° characterized by a red-shift in the UV-vis spectrum relative to the monomer [11–13]. From UV-vis spectral analysis based on Kasha exciton theory [8–10], simply the approximate tilt angle for accumulation of N molecules can be calculated according to the following equation,

$$\Delta\nu = 2\frac{N-1}{N}\cdot\frac{<m^2>}{h\cdot r^3}(1-3\cos^2\alpha) \tag{1}$$

$$\left\langle \mathrm{m}^2 \right\rangle = 9.185\times10^{-39}\int_{\lambda_1}^{\lambda_2}\varepsilon(d\lambda/\lambda) \tag{2}$$

where Δν is the spectral shift from the monomer absorption; h is the Planck's constant; r is the separation of centers; α is the tilt angle between the line of center and molecular long axes; $<m^2>$ refers to the transition dipole moment of monomer; ε aims at the molar extinction coefficient in $(\text{moles/L})^{-1}\,\text{cm}^{-1}$; λ is the wavelength; and λ_1 and λ_2 are the limits of a well-defined absorption band. This theory has been successfully applied to determine the J-aggregation of small organic molecules, such as perylene [11], assembled on pipe inner wall of AAO templates. This is further discussed below.

Further, in light of the molecular exciton theory, Akins [39] reported a study on Raman scattering enhancement theory for a finite aggregate structure consisting of N molecules, assuming the formation of molecular vibro-excitonic levels. The quantum mechanical Hamiltonian describing the internal system of the N molecules can mutually interact through a potential term V, which was given by [39],

$$\mathrm{H} = \sum_{n=1}^{N}\left(H_n + \sum_{m>n}V_{nm}\right) \tag{3}$$

where H is the Hamilton operator of kinetic energy; and V_{nm} refers to the interaction potential of molecules n and m (m is any of the other molecules taken together with molecule n). Thus for an individual molecule n, the vibronic wave function can be given by [39],

$$\varphi_{nj}(\rho,\mathrm{Q}) = \varphi_n(\rho,\ Q_0)x_{ni}(Q) \tag{4}$$

here n aims at the position of the probe molecule and j refers to a composite quantum number corresponding to the number of vibrational quanta of excitation. The character ρ is a composite spatial coordinate of the electrons, Q is the normal coordinate, and Q_0 represents the normal coordinates for the ground-state equilibrium configuration.The function φ refers to a multiple

electron wave function depending on the coordinates and spins of the electrons, while x corresponds to the vibrational wave function. Based on Born-Oppenheimer approximation, the normalized vibro-exciton wave function can be ascertained and thus the allowed energies. Further, according to the theory by Craig and Thirunamachandra [40], the Raman scattering intensity in a particular direction can be given by [39],

$$I(k') = \frac{\tilde{N} I_{k'}{}^4}{16\pi\varepsilon_0{}^2} \left| \sum_r \left\{ \frac{(\vec{\mu}^{mr} \cdot \vec{e}')(\vec{\mu}^{r0} \cdot \vec{e})}{E_{r0} - \hbar ck} + \frac{(\vec{\mu}^{mr} \cdot \vec{e})(\vec{\mu}^{r0} \cdot \vec{e}')}{E_{r0} + \hbar ck'} \right\} \right|^2 \tag{5}$$

where $\tilde{N}$ is the number of scattering centre; $\vec{\mu}$ is transition dipole moment vector; $\vec{e}$ is microscopic electric field strength vector; and E_{r0} shows the energy difference between the upper excited state r and the ground state 0. From first-order perturbation theory, the Raman scattering of aggregated molecules can be expressed as [39],

$$\lambda_{rs}(Q) = (\sum_\alpha h_{rs}{}^\alpha Q_\alpha)(\Delta E_{rs}{}^0)^{-1} \tag{6}$$

in which $h_{rs}{}^\alpha$ is a coupling term between electronic states r and s for the molecule with equilibrium ground-state configuration [39]. This theory has been successfully applied to dye molecules that form ground-state and excited-state aggregation structures, where an intrinsic enhancement was often gained on the formation of aggregates containing N monomers [39, 41].

3. Plasmon-free Raman scattering of molecule aggregates

Raman scattering of molecule aggregates, held together by dispersion and electrostatic forces, has been found different from that of non-aggregated monomers and bulk crystals. Moreover, the Raman bands observed for the aggregates could shift from those of the isolated monomers depending on the intermolecular interactions (i.e., strong or weak; covalent or non-covalently coupled interactions). This characteristic enables Raman spectroscopic studies of molecule aggregates to determine phase transition and photo-assisted polymerization. It is worth noting that, upon resonant excitation, the excited states often bring forth new Raman bands associated with lattice motions, e.g., typical motions in the aggregate formation direction. In this section, we emphasize on a few examples of normal Raman investigations of molecule aggregates.

3.1. To determine phase transition

It has been widely recognized that the assembly of target molecules can result in novel responses of Raman spectroscopy. For example, when examining Raman spectra of barium dialkyl phosphates at various chain lengths, Okabayashi et al. [42] found that the PO_2^-

symmetric stretching mode of dipentyl phosphate appears at 1106 cm^{-1} for the liquid crystal state formed at room temperature, which differs from that in the aqueous solution (ca. 1075 cm^{-1}). Also found was that, the relative intensities of the Raman spectral lines changed sharply at the phase-transition temperature but were found to be a constant below and above the transition point. By fully examining the Raman intensities and Raman shifts of the PO_2^- symmetric-stretching modes of dipentyl phosphate (1075 cm^{-1}), diester O-P-O and dibutyl phosphate (at 1090 and 1068 cm^{-1}), phase transition and the coexistence of two types of aggregation structures were determined. These Raman investigations illustrated how cation-phosphate interactions are important to form aggregation structures and affect the phase transition in liquid crystals of dialkyl phosphates.

3.2. Aggregation-enhanced Raman scattering (AERS)

A few meticulous investigations dealing with relative Raman intensities and selection rules for aggregates have demonstrated a concept termed "aggregation-enhanced Raman scattering" (AERS) [43], which was proposed to represent a concept solely for studies of aggregates, which differs from a mechanism based on SERS, resonance Raman scattering, and Mie scattering since these Raman effects ignore the impact of aggregation of molecules. The aggregation of molecules in their ground state may result in enhanced polarizability compared to monomeric species and hence intensified radiation according to the basic principle for a dipole moment $\mu = \alpha E$, where α is the polarizability and E is the coupled field. On the other hand, the aggregates could form molecular excitonic states allowing for a coupling effect (between excitonic states) which alters the cross-section of Raman scattering, because the participation of more energetic states readily gives rise to an enhanced response to incident radiation [43]. In this point, resonance Raman scattering, where the incident exciton overlaps a small number of exciton bands, is expected to result in further enhancement of vibrational bands. Akins have conducted numerous investigations relating to AERS [41, 44–54], as partly included in a recent review article [43].

3.3. Resonance Raman effect from aggregation

Resonant Raman spectroscopy (RRS) has been known as a main enhancement strategy to solve the sensitivity issue and to derive Raman labels for applications. For example, Zajac et al. [23] reported an interesting study on aggregation-induced resonance Raman optical activity (AIRROA) of astaxanthin (3,3′-dihydroxy-β,β-carotene-4,4′-dione, AXT), a chiral xanthophyll that was known to bear high antioxidant potency beneficial to cardiovascular, inflammatory, immune and neurodegenerative diseases. Along with striking differences of UV-vis spectra of the monomer and aggregates, Raman spectra (**Figure 1**) demonstrated spectral changes (e.g., 5 cm^{-1} blue-shift of the C═C stretching mode, and the appearance of a new band at ~280 cm^{-1}) due to J-aggregation of astaxanthin along with a quenched fluorescence background. Considering the fact of low sensitivity determined by the main limitation of Raman optical activity (c.a., approximately one photon in a billion), resonance effect and aggregation enhancement is important to further advances of AIRROA investigations.

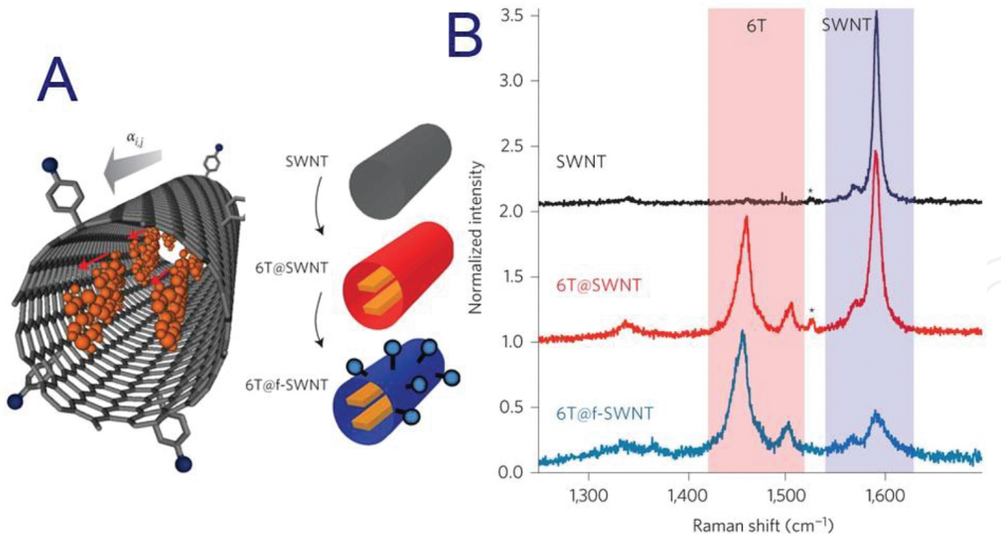

Figure 1. (A) A schematic representation of the 6T@f-SWNT with bromophenyl groups grafted onto its sidewall, and description of the encapsulation and chemical functionalization steps to prepare the α-sexithiophene encapsulated inside a covalently functionalized SWNT (6T@f-SWNT). (B) Raman spectra at λ = 532 nm excitation of an individual SWNT, α-sexithiophenes (6T) inside a SWNT (6T@SWNT) and after the covalent functionalization step (6T@f-SWNT). The polymer monoliths composed Ref. [55].

Recently, Gaufrès et al. [55] reported an interesting study on encapsulated and aggregated dye molecules inside single-walled carbon nanotubes [55], where giant Raman scattering effect was discovered. Raman measurements for the rod-like dyes (α-sexithiophene and β-carotene) assembled in single-walled carbon nanotubes exhibit highly-polarizable J-aggregates, as shown in **Figure 1**, giving an enhanced resonant Raman cross-section above that required for detecting individual aggregates. It was found that the shielding of carbon nanotube enables fluorescence-free background and photobleaching-free Raman signals, allowing the giant Raman effect used as functionalized nanoprobe labels for Raman imaging with robust detection using multispectral analysis. Beside this, there are also a few other interesting research papers dealing with Raman scattering by encapsulated molecules in carbon nanotubes, where the formation of aggregates give rise to well-resolved Raman spectra due to interaction and charge transfer within the carbon nanotubes [56, 57].

3.4. Magnetic field-trapped Raman scattering

The exploration of magnets and magnetism is associated with human history. Recently, Luo et al. [37] reported an interesting photo-assisted method to magnetize microcrystal fullerene C_{60} at room temperature by exciting C_{60} molecules to triplet states via proper laser radiation and then trapping the spin-polarized states under a strong magnetic field (**Figure 2**). Raman spectroscopy was found an operative probe due to its fingerprint spectra regarding energy levels and molecular states, and the crystalline form of C_{60} molecule aggregates is held together by van der Waals forces allowing the conversion to polymeric phase under proper laser radiation [58]. As results, novel changes on Raman scattering of micro-crystal solid C_{60} were discovered in the presence and absence of the magnetic field; also found was that the Raman

spectra exhibited "hysteresis" phenomenon when the external magnetic field was removed. Together with first-principles calculations which well reproduced the Raman activities of C_{60} on different states [37], as seen in **Figure 2**, photo-assisted magnetization (PAM) of the fullerenes and magnetic-field trapped Raman spectroscopy (MFTRS) were proposed [37]. The PAM strategy with MFTRS verification opens a new approach and, as a general protocol, enables the magnetization of common materials that consist of only light elements. The importance of spin-spin and spin-orbit interactions was also demonstrated in nano-graphene fragments [59]; Raman spectroscopy also plays an important role in identifying single- and few-layer graphene [60, 61].

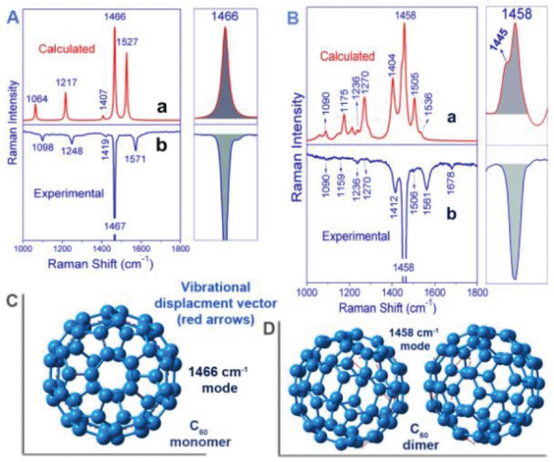

Figure 2. (A) Calculated Raman activity of a singlet-state C_{60} monomer (a), comparison of a normal FT-Raman spectrum of solid C_{60} (b); (B) calculated Raman spectrum of a quintet-state dimer C_{60} (a), compared with the 514.5-nm Raman of solid C_{60} in the presence of a B = 2.5 T magnetic field (b); (C and D) The strongest vibrational modes of a singlet-state C_{60} monomer (1466-cm^{-1}) and a quintet-state C_{60} dimer (1458-cm^{-1}). The displacement vectors are shown with red arrows.

3.5. Raman probes for aerosols

Raman spectroscopy is useful in characterizing atmospheric aerosols profiting from the development of portable Raman instrument in recent years [62–77]. For example, Aggarwal et al. [77] developed a Raman spectrometer using 532-nm continuous wave laser and used for detecting and identifying chemical aerosols of a low-concentration in atmospheric air. As results, they demonstrated the successful application of Raman for trace detection and analysis of iso-vanillin aerosols up to a mass concentration of 1.8 ng/cm^3 with the signal-to-noise ratio at about 19 in 30s for the 1116-cm^{-1} mode with a decent Raman cross section of 3.3×10^{-28} cm^2 at the use of 8-W double-pass laser power. Among others, Batonneau et al. [78] reported an interesting study on heterogeneous chemistry of aerosol particles utilizing Raman mapping and spectroscopic method, which was found in agreement with elemental images obtained by X-ray-mapping. An et al. [79] conducted a systematic study to identify a few typical organic compounds (isoprene, terpenoids, pinenes etc.) which are known as the main sources of organic aerosols (OAs) particle matter in air pollution. Raman and IR spectra of isoprene,

terpenoids, pinenes and their mixtures were examined showing distinguishable vibrational spectroscopic fingerprints of the three components respectively. It was noted that, in a certain case such as β-pinene, a dimer model reproduces the experimental results other than single molecule modeling, indicating nonneglectable intermolecular interactions and aggregation states for aerosols challenging the present mechanisms based on single molecule theory. Further, Raman spectra from an ambient sample can be analyzed using a hierarchical clustering method to check out whether the spectra of aerosols in consistence with relating organic compounds. In particular, analysis on time-resolved aerosol Raman spectra over the course of several hours, simply by checking the D-G bands of amorphous carbon plotted vs time (e.g., a half-hour intervals), enables to monitor and judge the increase/decrease of related pollution in atmosphere [78, 80, 81].

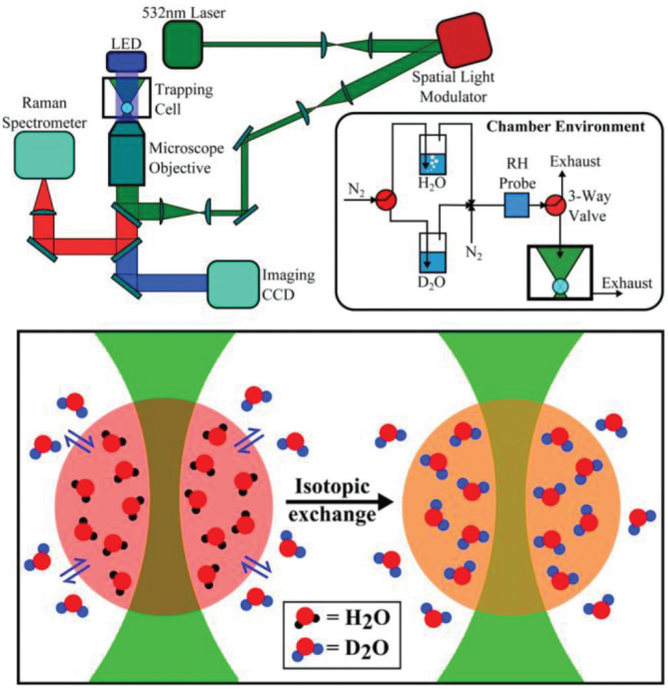

Figure 3. (Top) Standard optical tweezers (Biral AOT 100) arrangement. (Inset) Valve system used to initiate exchange between D_2O and H_2O. (Bottom) A sketch showing isotopic water diffusion in aerosol by the use of optical tweezers. Reproduced with permission from Ref. [71].

Recently, Davies and Wilson [71] employed an aerosol optical tweezer technique for contactless levitation of single droplets (e.g., 3–6 μm in radius) and then for Raman investigations, as shown in **Figure 3**. Flexible environmental control system allows for rapid exchange of the gas-phase humidity source between H_2O and D_2O (**Figure 3**) to monitor the progression of the droplet composition using Raman spectroscopy. Utilizing a model describing diffusion in a sphere (i.e., solution to Fick's second law), they analyzed the data by varying diffusion coefficients (D_w) in viscous media to achieve the best fit to both D_2O and H_2O data sets. This droplet-based isotopic tracer method takes a few advantages for measurement of diffusion coefficients. The resolution of gel formation suggests promising application to identify phase

behavior that leads to abrupt changes in water mobility (e.g., hydrophobic phase separation, aerosol formation and rapid growth), enabling to explore the changing role of water diffusion at chemical transformation thus valuable insights into the oxidative aging behavior in determining diffusive properties of atmospheric aerosol.

4. SERS systems involving molecule aggregates

Besides normal Raman, abundant SERS investigations have been undertaken by employing thin films of analytes on functional substrates, such as the extensive investigations of Raman and SERS from Langmuir-Blodgett (LB) films which are often associated with intermolecular interactions of aggregates [82–89]. One of the advantages is that the uniform sampling of thin films allows for better signal-to-noise of the SERS spectra from the analytes [82, 86]. Besides extensive investigations of such 2D assemblies of "analytes + nanoparticles" into thin films, previous publications also addressed 1D assemblies of molecular aggregates (analytes) and metal nanoparticles (signal amplifier).

4.1. Template-based uniform assembly

Considering that Raman/SERS measurements at different positions of the samples could take on diversity due to molecule orientation and disorder degree, location and/or "hot-spots" dependence, the uniformity of molecular aggregates or SERS substrate is largely desired in order to get a better averaged collection of Raman signal. Anodic aluminum oxide (AAO) membrane is widely utilized as a versatile template to prepare 1D rodding/tubing and 2D nanoarray ordered structures, [90–95] both of which have found applications to SERS investigations. On one hand, AAO templates are ideal sublayers to filtrate and support noble metal nanoparticles hence forming highly SERS-active systems [96–98]. For another, AAO templates were also utilized to assemble organic molecules (e.g., perylene) for SERS investigations [11], as shown in **Figure 4**(left), where highly-ordered arrays of core-shell nano-pillars of Ag-perylene were fabricated simply by preparing perylene nanotubes utilizing the versatile AAO template [13], and followed by an electrochemical deposition of Ag [11]. Well-resolved Raman spectra with very good signal-to-noise background were obtained for the perylene (originally a large fluorescence yield) at an UV-vis excitation, profiting from the uniform assembly of perylene molecules. Based on the aforementioned theory and Eqs. (1) and (2), it was estimated that the molecular tilt angle is less than 54.7° indicating a head-to-tail J-aggregation of the perylene molecules along the inner walls of the AAO pores [11]. Similarly, high-quality SERS spectra of fullerene C_{60}/C_{70} were also obtained from ordered arrays of core-shell nano-pillars of $Au@C_{60}/C_{70}$, as shown in **Figure 4**(right) [99]. These results evidenced that coincident and uniform assembly of fullerene molecules along the Au nano-rods leads to fluorescence quenching, and the ordered arrays of nano-pillars generate enhanced LSPR and hence remarkable SERS effect up to 10 times of signal amplification compared to the usual SERS results.

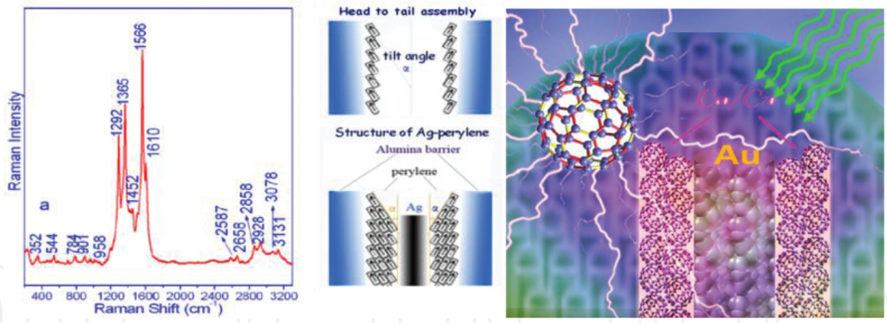

Figure 4. (Left) SERS spectrum of perylene from the standing Ag-perylene core-shell nano-pillars array; (middle) a sketch of the assembly of perylene molecules loaded with Ag as the core; (right) a sketch map showing the Au@C_{60}/C_{70} nanopillars.

4.2. Assemblies of "analytes + nanoparticles"

By utilizing porous polymer monoliths functionalized with Ag nanoparticles as media, Liu et al. [100] showed a SERS system with assembly of the analyte molecules, as shown in **Figure 5**. The polymer monoliths composed of porous 3D-structured organic materials were prepared from monomers with unsaturated vinyl groups [101]. The monoliths could have μm- to nm- sized tortuous fluidic channel networks which enable the convection flow for rapid mass transfer while shorten the characteristic diffusion length. Compared to usual colloidal SERS systems, the monolith was demonstrated to concentrate the embedded metal nanoparticles and present a tremendous amount of surface area and more interaction between the analyte and Ag nanoparticles [100].

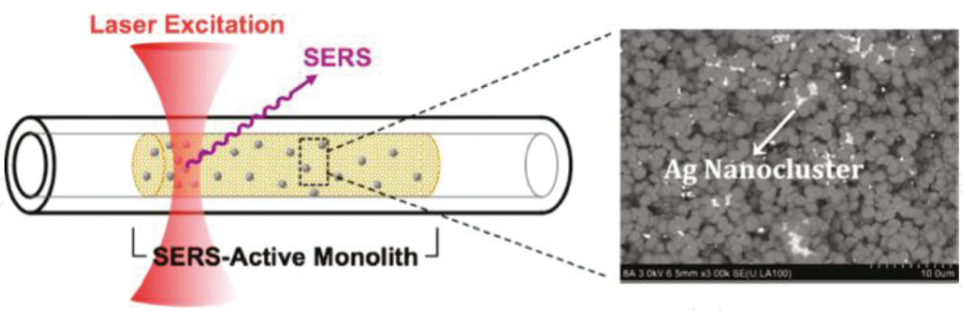

Figure 5. A sketch for the nanoparticle-functionalized porous polymer monolith detection elements for SERS investigations. Reproduced with permission from *Anal. Chem.* 2011 [100].

The one-dimensional assembly of "analytes + nanoparticles" may not need any supports or templates. For example, Z. Luo found that, micro-fiber assembly of organic molecules such as 2,2′-bipyridyl (22BPY) can be formed by directly injecting saturated solution of the target molecules into ice-cold Ag colloid [22]. This strategy was demonstrated to resemble a reprecipitation method (or named as microfluidic technique) which was widely used to prepare size-controlled organic nanostructures [102]. As shown in **Figure 6**, the high-quality spectrum

suggested that the microfiber assemblies of 22BPY combined with Ag nanoparticles are a highly SERS-active systems differing from SERS of individuals [22].

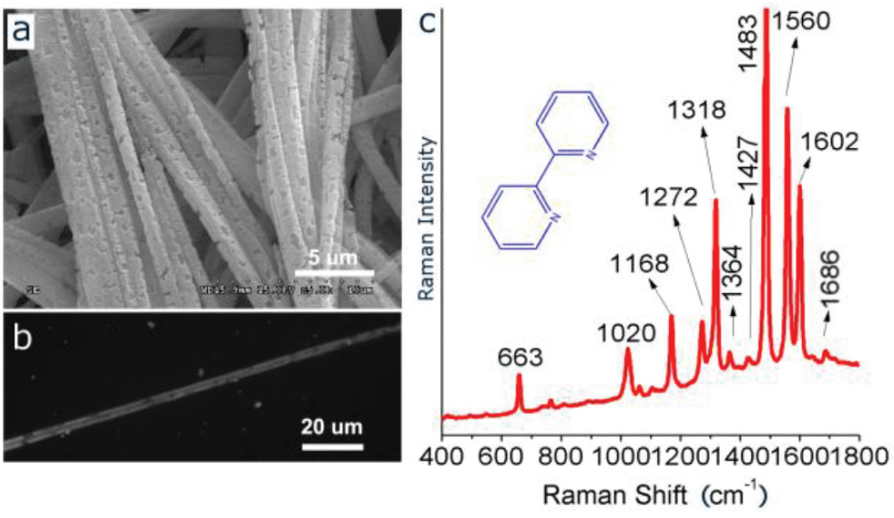

Figure 6. (a) A SEM image of 22BPY microfibers via reprecipitation method by injecting saturated 22BPY solution into ice-cold Ag colloid, (b) microscopy bright-field image of a single fiber, and (c) correlative micro-Raman spectrum measured from this microfiber of 22BPY.

4.3. On-the-specimen method

As a powerful technique for trace analysis and detection due to the extremely high sensitivity and rich structural information that it can offer, SERS has been extensively investigated not only on the primal three classes of SERS systems (i.e., metal colloids, electrodes, and island films), but also non-traditional substrates [103–105]. For example, SERS studies involving surface coatings of Ag/Au nanoparticles, as named *on-the-specimen* method, have been largely applied in identification for art conservation, especially cultural relics and archeology [38, 106]. In general, the colorant components comprised of inorganic salts can be identified using normal Raman spectroscopic measurements, but strong fluorescence of organic dyes often precludes Raman measurements. SERS fulfills the requirements of an ideal analytical technique to detect and identify colorants and organic dyes in artworks [107–109]. In a few typical investigations such as those by Brosseau et al. [110, 111] examination on the samples of actual historical textiles, pastels, and watercolors, etc. have been conducted revealing the unique advantages of SERS sensitivity and providing distinguishable information available for long term preservation. Recently utilizing bubbling gas strategy for laser ablation in liquid (LAL), Luo et al. [112] prepared chemically-pure gold clusters for a practical use of discrimination among different surfaces, as demonstrated the identification of various documents from different printers/copiers and written with different pen-inks, as shown in **Figure 7** [112]. These investigations pertaining to molecule aggregation states give important application of Raman/SERS spectroscopy within a minimally-invasive manner [112].

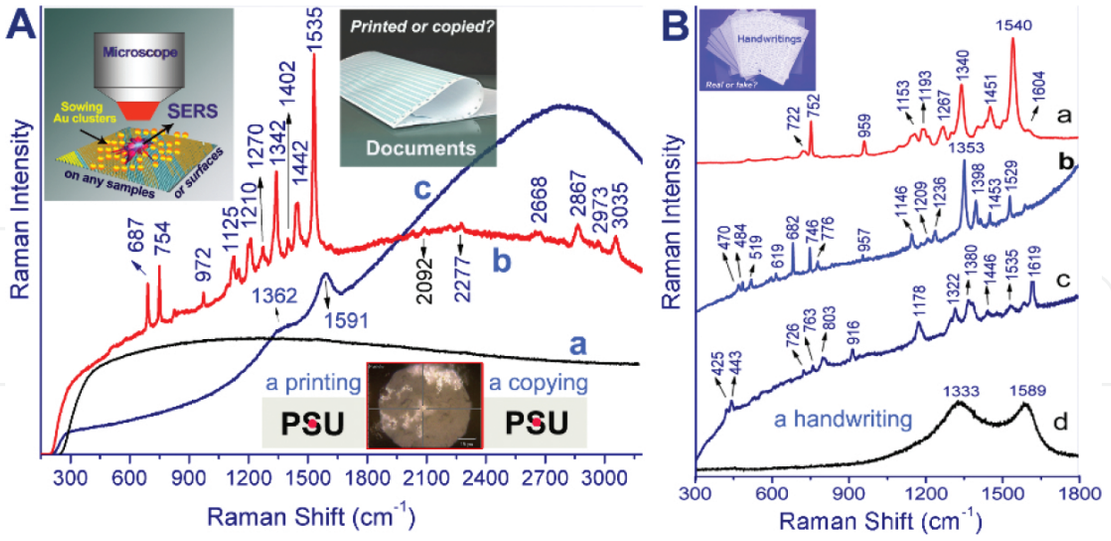

Figure 7. (A) Undistinguishable Raman of a "PSU" document from both a printer and a copier (a); SERS spectrum of the document from the printer (Xerox Phaser 8560DN PS, Genuine XEROX Solid Ink, black) (b), compared with that from a copier (RICOH, Aficio, MP 7001) (c). (B) SERS examination of four handwritten samples, by coating the gold clusters on the ink-area.

Recently, Tian et al. have further pullulated this method in help of shell-isolated nanoparticle-enhanced Raman scattering (SHINERS) technique [113, 114], as sketched in **Figure 8**. For a typical SHINERS system, Au nanoparticles were coated with ultrathin silica shells and sowing on probed surfaces, where the Au core provides SERS signal enhancement while the silica shell shields the metal core from direct contact with analyte molecules (i.e., prevents the contamination of the chemical system under study) [115], which differs from general SERS sampling method, simply by adding analytes onto SERS-active substrates or directly mixing the target solution with metal colloids [115–118]. The SHIERS 'smart dust' on the analyte surfaces was demonstrated of practical use in a few interdisciplinary research fields, such as inspecting pesticide residues on food and fruit, examining drug security and environment protection accurately and rapidly, and characterizing biological structures.

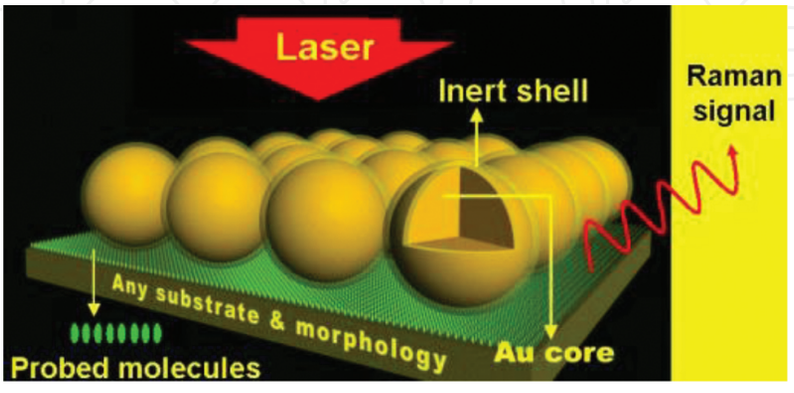

Figure 8. A sketch showing the in-situ probing of biological structures by SHINERS. Reproduced with permission from *Nature* 2010. [61, 62]

http://dx.doi.org/10.5772/66098

5. Raman investigations of cluster systems

5.1. Raman scattering of gas-phase clusters

Raman spectroscopy can also provide essential vibrational information of clusters, although only a few investigations have been published so far. For this study, coherent anti-Stokes Raman spectroscopy (CARS) takes advantages of its excellent sensitivity as applied to investigations of isolated water clusters [119–121], but the nonlinearity of CARS experiments remains a challenge to the assignment of cluster sizes and structure identification. It is worth mentioning that Raman activity of gas-phase clusters is associated with free-rotating especially at high temperature, thus the internal rotational motions could largely differ from that obtained by matrix-assisted vibrational spectroscopic measurements where the molecule/clusters could be partially or wholly clamped. Among others, Otto et al. [122] reported a study of cold water oligomers utilizing spontaneous Raman scattering (SRS) technique and revealed the vibrational dynamics of water molecules, as shown in **Figure 9**. Analysis of Raman and IR activities of the hydrogen bond-mediated water clusters seeded in rare-gas expansion molecule beam provides insights into the excitonic OH oscillator coupling, as well as vivid information of ultrafast intermolecular energy transfer (which was often suppressed in femtosecond experiments for the condensed phase due to isotopic dilution). Such investigations from gas-phase chemistry enable to determine weakened or intensified Fermi resonance between OH-stretching and OH-bending motion of hydroxide radicals.

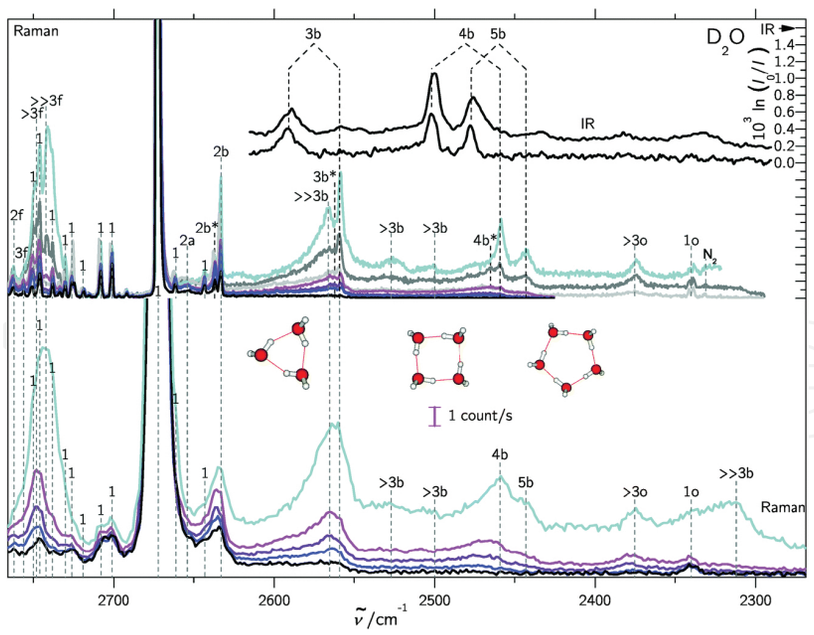

Figure 9. Raman and IR spectra of mixed D_2O/rare gas expansions. Raman spectra were scaled to the same monomer scattering intensity at the point of measurement in the respective blocks. Lower part: Raman spectra recorded using a 0.5 m monochromator. Basically, the clustering extent increases from bottom to top. Upper part: similar conditions but recorded using a 1 m monochromator. The clustering extent increases from bottom to top. Reproduced with permission from Ref. [122].

5.2. Raman scattering from monolayer-protected clusters

While expanded Raman investigations of gas-phase clusters remain a reasonable challenge, there are several publications addressing the Raman activities of monolayer-protected clusters (MPCs). Considering that the mid infrared region of the spectrum mainly reveals information about the ligand structures (e.g., C—H, N—H, O—H bond etc.) and their interactions with the metal core [123, 124], Raman spectroscopy actually has its advantages to identify low frequency vibrational modes such as S-Au-S stretching, wagging, scissoring, rocking, and twisting. These vibrations are expected to be weak in IR spectrum due to the low polarity (i.e., IR non-active) but likely prominent in the Raman spectrum (i.e., Raman active) [125, 126]. **Figure 10** presents a typical example of Au_{38} and Au_{25} MPCs, where the vibrations of two clusters containing monomeric (SR-Au-SR) and dimeric (SR-Au-SR-Au-SR) gold-thiolate staples in the metal-ligand interface are addressed. Raman activities of these clusters at different charge state with different protection ligands illustrated influences of cluster sizes and composition with respect to the monomeric and dimeric moieties [127].

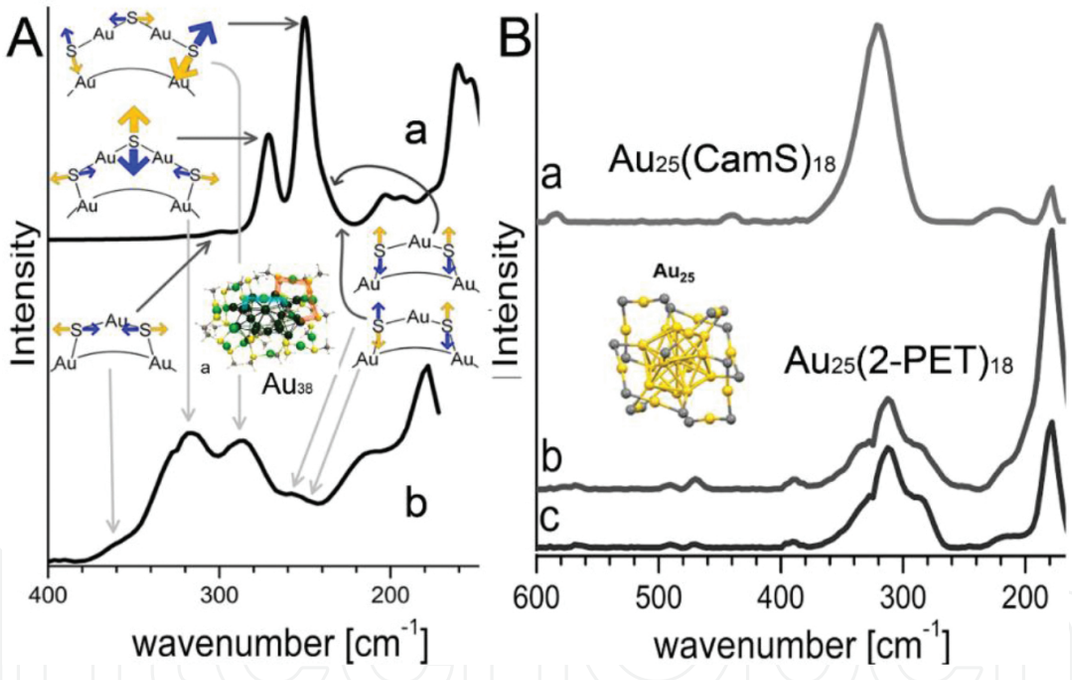

Figure 10. (A) Calculated (a) and experimental (b) Raman spectrum of the $Au_{38}(SCH_3)_{24}$ and $Au_{38}(2\text{-PET})_{24}$ cluster, respectively. The experimental spectrum is cut off at 170 cm^{-1}, the cutoff point of our optical filter. Radial and tangential Au–S modes of the staples are schematically represented. Radial vibrations of the long staples are responsible for bands with high intensity. Modes associated with the short staples (symmetric and antisymmetric stretching and tangential vibrations) have lower Raman intensity. (B) RCF-corrected Raman spectra of the low-frequency region of $Au_{25}(CamS)_{18}$ (a), $Au_{25}(2\text{-PET})_{18}^{0}$ (b), and $Au_{25}(2\text{-PET})_{18}^{-}$ (c). The clusters were measured coated on a rotating glass slide. Reproduced with permission from Ref. [127].

In addition to the small number of experimental Raman investigations of clusters, there are vast theoretical studies relating to cluster systems [128–136]. For example, utilizing time-dependent density functional theory (DFT) calculations, Chen et al. [137] conducted a detailed Raman study of pyridine adsorbed on $M@Au_{12}$ and $M@Ag_{12}$ (M = Mo, W) clusters. They found

http://dx.doi.org/10.5772/66098

that, the calculated Raman intensity of pyridine on $M@Ag_{12}$ at charge transfer (CT) transition excitations were twice as that for pyridine on $M@Au_{12}$, as shown in **Figure 11**, and the energies used for SERS excitations (in the region of 1.63–2.10 eV) were largely different from each other. Calculated interactions between the core and shell produced varying and strong CT transitions from the metal clusters to pyridine, which was demonstrated to be responsible for the altered optical properties. Also found was that, the complexes of pyridine on silver-caged clusters are largely tunable with the core compared to gold-caged clusters, providing insights to the silver and gold clusters even at the same sizes.

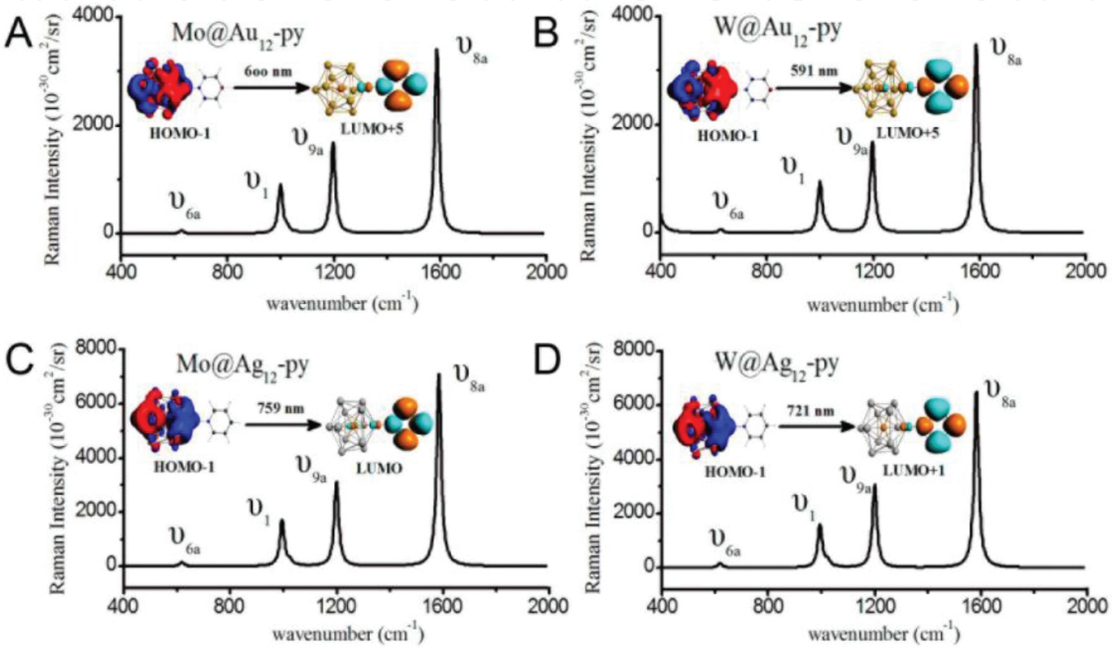

Figure 11. Raman spectra with CT excitation of the (A) $Mo@Au_{12}$-Py complex, (B) $W@Au_{12}$-Py complex, (C) $Mo@Ag_{12}$-Py complex, and (D) $W@Ag_{12}$-Py complex. Differential cross sections are in units of 10^{-30} cm^2/sr and wavenumbers are in cm^{-1}. Spectra have been broadened by a Lorentzian having a width of 20 cm^{-1}. Reproduced with permission from Ref. [137].

Regarding to the interesting CT of silver cluster with small organic molecules, recently Chen et al. [138] have given a study to the interactions between tetracyanoquinodimethane (TCNQ) and two typical silver clusters Ag_{13} and Ag_{20}, as shown in **Figure 12**. It was found that charge transfer from silver clusters to TCNQ molecules initiates the Ag—N bond formation at selective sites giving rise to different isomers of the Ag_{13}-TCNQ and Ag_{20}-TCNQ complexes. From a spectroscopic analysis for the two CT complexes mainly on Raman and infrared activities, vivid illustration of electron cloud interactions and the behavior of TCNQ adsorbed on silver clusters was comprehensively demonstrated, along with frontier molecular orbital (FMO) and natural bond orbital (NBO) patterns. The calculated Raman activity for a TCNQ molecule of Ag_{20} was found consistent with experimental Raman measurement of TCNQ molecules on single-crystal Ag(1 1 1) surface. Further efforts in this field regarding to clusters and complex molecular aggregates are expected to clarify the charge-transfer interactions within building blocks of granular materials [138–140].

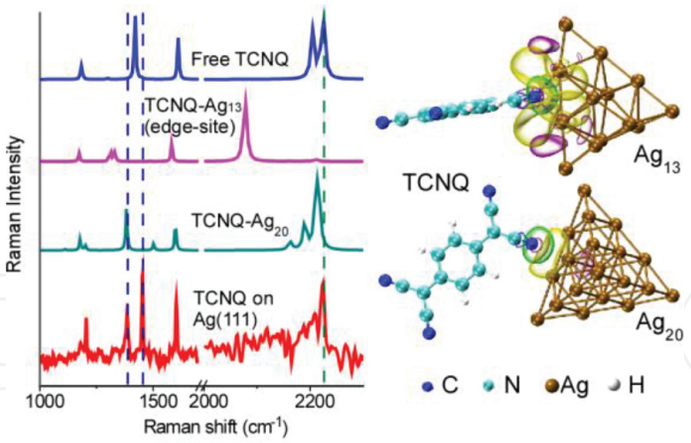

Figure 12. (Left) Raman spectra of TCNQ molecules. Calculated spectra of a free TCNQ molecule (blue, top) and surface-adsorbing Ag_{13}-TCNQ (purple) Ag_{20}-TCNQ (green) complexes; and experimental spectra of TCNQ on Ag(1 1 1) surface of silver single crystal (red).Interactions of tetracyanoquinodimethane with silver clusters Ag_{13} and Ag_{20} are demonstrated by first-principles calculations and Raman/IR spectroscopy. (Right) Natural bond orbital (NBO) donor-acceptor (overlap) interactions between N and Ag atoms in Ag (cluster)-TCNQ complexes.

6. Conclusions

In this chapter, Raman spectroscopy is demonstrated of importance in solving scientific issues relating to molecule aggregates and cluster systems profiting from its spectral fingerprints by which aggregation states, phase transition and cluster structures can be identified. Raman theory for aggregated molecules is simply introduced based on molecular exciton theory and Raman scattering enhancement at the formation of vibro-excitonic levels. Next, we summarize the research advances toward both plasmon-free Raman and SERS systems, such as aggregation-enhanced Raman scattering (AERS), resonance Raman (RR) effect from aggregation, magnetic-field trapped Raman scattering (MFTRS), shell-isolated nanoparticle-enhanced Raman scattering (SHINERS), and Raman probes for aerosols, etc. With the development of scientific instrumentation, the importance of Raman spectroscopy toward precise-sized molecule aggregates and cluster systems will be more clearly embodied, enabling to step toward interdisciplines of cluster science, molecular science, material science and surface science.

Author details

Zhixun Luo* and Jiannian Yao

*Address all correspondence to: zxluo@iccas.ac.cn

Institute of Chemistry, Chinese Academy of Sciences, Beijing, China

References

[1] Jayakannan, M. Probing the π-stacking induced molecular aggregation in π-conjugated polymers, oligomers, and their blends of -phenylenevinylenes. *J. Phys. Chem. B* 2008, *112*, 1119–1129.

[2] Hu, R.; Feng, J. A.; Hu, D. H.; Wang, S. Q.; Li, S. Y.; Li, Y.; Yang, G. Q. A rapid aqueous fluoride ion sensor with dual output modes. *Angew. Chem. Int. Ed.* 2010, *49*, 4915–4918.

[3] Chen, J. W.; Law, C. C. W.; Lam, J. W. Y.; Dong, Y. P.; Lo, S. M. F.; Williams, I. D.; Zhu, D. B.; Tang, B. Z. Synthesis, light emission, nanoaggregation, and restricted intramolecular rotation of 1,1-substituted 2,3,4,5-tetraphenylsiloles. *Chem. Mater.* 2003, *15*, 1535–1546.

[4] Knapp, E. W. Lineshapes of molecular aggregates, exchange narrowing and intersite correlation. *Chem. Phys.* 1984, *85*, 73–82.

[5] Fidder, H.; Knoester, J.; Wiersma, D. A. Optical properties of disordered molecular aggregates: numerical study. *J. Chem. Phys.* 1991, *95*, 7880.

[6] Davydov, A. S.: *Theory of molecular excitons*; Plenum Press: New York, 1971.

[7] Köhn, S.; Kolbe, H.; Korger, M.; Köpsel, C.; Mayer, B.; Auweter, H.; Lüddecke, E.; Bettermann, H.; Martin, H. D.: Aggregation and interface behaviour of carotenoids. In *Carotenoids: Volume 4: Natural Functions*; Britton, G., Liaaen-Jensen, S., Pfander, H., Eds.; Birkhäuser Basel: Basel, 2008; pp. 53–98.

[8] Kasha, M.; Rawls, H. R.; EI-Bayoumi, M. A. The exciton model in molecular spectroscopy. *Pure Appl. Chem.* 1965, *11*, 371–392.

[9] Davydov, A. S.: *Theory of molecular excitons*; McGraw-Hill: New York, 1962.

[10] Kasha, M. Relation between exciton bands and conduction bands in molecular lamellar systems. *Rev. Mod. Phys.* 1959, *31*, 162–169.

[11] Luo, Z.; Peng, A.; Fu, H.; Ma, Y.; Yao, J. N.; Loo, B. H. An application of AAO template: orderly assembled organic molecules for surface-enhanced Raman scattering. *J. Mater. Chem.* 2008, *18*, 133–138.

[12] Katoh, T.; Inagaki, Y.; Okazaki, R. Synthesis and properties of bismerocyanines linked by a 1,8-naphthylene skeleton. Novel solvatochromism based on change of intramolecular excitonic coupling mode. *J. Am. Chem. Soc.* 1998, *120*, 3623–3628.

[13] Zhao, L.; Yang, W.; Ma, Y.; Yao, J.; Li, Y.; Liu, H. Perylene nanotubes fabricated by the template method. *Chem. Commun.* 2003, 2442–2443.

[14] James, T. H.: *The theory of the photographic process*; Macmillan: New York, 1977.

[15] Infelta, P. P. Fluorescence quenching in micellar solutions and its application to the determination of aggregation numbers. *Chem. Phys. Lett.* 1979, *61*, 88–91.

[16] Almgren, M.; Lofroth, J. E. Determination of micelle aggregation numbers and micelle fluidities from time-resolved fluorescence quenching studies. *J. Colloid Interface Sci.* 1981, *81*, 486–499.

[17] Alargova, R. G.; Kochijashky, II; Sierra, M. L.; Zana, R. Micelle aggregation numbers of surfactants in aqueous solutions: a comparison between the results from steady-state and time-resolved fluorescence quenching. *Langmuir* 1998, *14*, 5412–5418.

[18] Ma, X.; Sun, R.; Cheng, J.; Liu, J.; Gou, F.; Xiang, H.; Zhou, X. Fluorescence aggregation-caused quenching versus aggregation-induced emission: a visual teaching technology for undergraduate chemistry students. *J. Chem. Educ.* 2016, *93*, 345–350.

[19] An, B. K.; Kwon, S. K.; Jung, S. D.; Park, S. Y. Enhanced emission and its switching in fluorescent organic nanoparticles. *J. Am. Chem. Soc.* 2002, *124*, 14410–14415.

[20] Li, S. Y.; He, L. M.; Xiong, F.; Li, Y.; Yang, G. Q. Enhanced fluorescent emission of organic nanoparticles of an intramolecular proton transfer compound and spontaneous formation of one-dimensional nanostructures. *J. Phys. Chem. B* 2004, *108*, 10887–10892.

[21] Luo, J. D.; Xie, Z. L.; Lam, J. W. Y.; Cheng, L.; Chen, H. Y.; Qiu, C. F.; Kwok, H. S.; Zhan, X. W.; Liu, Y. Q.; Zhu, D. B.; Tang, B. Z. Aggregation-induced emission of 1-methyl-1,2,3,4,5-pentaphenylsilole. *Chem. Commun.* 2001, 1740–1741.

[22] Luo, Z.; Loo, B. H.; Cao, X.; Peng, A.; Yao, J. Probing the conformational transition of 2,2′-bipyridyl under external field by surface-enhanced Raman spectroscopy. *J. Phys. Chem. C* 2012, *116*, 2884–2890.

[23] Zajac, G.; Kaczor, A.; Pallares Zazo, A.; Mlynarski, J.; Dudek, M.; Baranska, M. Aggregation-induced resonance Raman optical activity (AIRROA): a new mechanism for chirality enhancement. *J. Phys. Chem. B* 2016, *120*, 4028–4033.

[24] Pienpinijtham, P.; Han, X. X.; Ekgasit, S.; Ozaki, Y. An ionic surfactant-mediated Langmuir-Blodgett method to construct gold nanoparticle films for surface-enhanced Raman scattering. *Phys. Chem. Chem. Phys.* 2012, *14*, 10132–10139.

[25] Ostrovskii, D.; Kjoniksen, A. L.; Nystrom, B.; Torell, L. M. Association and thermal gelation in aqueous mixtures of ethyl(hydroxyethyl)cellulose and ionic surfactant: FTIR and Raman study. *Macromolecules* 1999, *32*, 1534–1540.

[26] Ma, C. X.; Harris, J. M. Surface-enhanced Raman spectroscopy detection of ionic solutes by surfactant-mediated adsorption to a hydrophobic surface. *Appl. Spectrosc.* 2013, *67*, 801–807.

[27] Gaufres, R.; Bribes, J. L.; Sportouch, S.; Ammour, J.; Maillols, J. Phase-transitions in non-ionic surfactant water-systems as studied by Raman spectrometry.2. A new methodology. *J. Raman Spectrosc.* 1988, *19*, 149–153.

[28] Cooney, R. P.; Barraclough, C. G.; Healy, T. W. Non-ionic surfactant structure in the liquid and micelle states—a Raman-spectroscopic study. *J. Phys. Chem.* 1983, *87*, 1868–1873.

[29] Wang, P.; Fu, L. M.; Zhang, J. P.; Kakitani, Y.; Ishii, H.; Nagae, H.; Koyama, Y. Strong carotenoid-to-peptide interaction immediately after triplet excitation triggering conformational changes in photo-reaction center-bound 15-cis-spheroidene as revealed by submicrosecond time-resolved Raman spectroscopy. *Chem. Phys. Lett.* 2008, *458*, 175–179.

[30] Okazaki, E.; Ito, A. Study on photo-reaction of maleimide derivatives using Raman spectroscopy. *Abstr. Pap. Am. Chem. Soc.* 2001, *222*, U312–U312.

[31] Ma, C. S.; Du, Y.; Kwok, W. M.; Phillips, D. L. Femtosecond transient absorption and nanosecond time-resolved resonance Raman study of the solvent-dependent photodeprotection reaction of benzoin diethyl phosphate. *Chem. Eur. J.* 2007, *13*, 2290–2305.

[32] Tireli, M.; Kulcsar, M. J.; Cindro, N.; Gracin, D.; Biliskov, N.; Borovina, M.; Curic, M.; Halasz, I.; Uzarevic, K. Mechanochemical reactions studied by in situ Raman spectroscopy: base catalysis in liquid-assisted grinding. *Chem. Commun. (Cambridge, U. K.)* 2015, *51*, 8058–8061.

[33] Oyama, S. T.; Zhang, W. True and spectator intermediates in catalysis: the case of ethanol oxidation on molybdenum oxide as observed by in situ laser Raman spectroscopy. *J. Am. Chem. Soc.* 1996, *118*, 7173–7177.

[34] Mazeikiene, R.; Niaura, G.; Malinauskas, A. In situ Raman spectroelectrochemical study of electrocatalytic processes at polyaniline modified electrodes: redox vs. metal-like catalysis. *Electrochem. Commun.* 2005, *7*, 1021–1026.

[35] Formo, E.; Wu, Z. L.; Mahurin, S.; Dai, S. In situ high temperature surface enhanced Raman spectroscopy study of catalysis. *Abstr. Pap. Am. Chem. Soc.* 2011, *241*.

[36] Dai, Z. G.; Xiao, X. H.; Zhang, Y. P.; Ren, F.; Wu, W.; Zhang, S. F.; Zhou, J.; Mei, F.; Jiang, C. Z. In situ Raman scattering study on a controllable plasmon-driven surface catalysis reaction on Ag nanoparticle arrays. *Nanotechnology* 2012, *23*, 335701.

[37] Luo, Z.; Cheng, X.; Luo, Y.; Loo, B. H.; Peng, A.; Yao, J. Photoassisted magnetization of fullerene C_{60} with magnetic-field trapped Raman scattering. *J. Am. Chem. Soc.* 2011, *134*, 1130–1135.

[38] Chen, J.; Ding, W.; Luo, Z.; Loo, B. H.; Yao, J. Probing single molecules and molecular aggregates: Raman spectroscopic advances. *J Raman Spectros.* 2015, n/a-n/a.

[39] Akins, D. L. Theory of Raman scattering by aggregated molecules. *J. Phys. Chem.* 1986, *90*, 1530–1534.

[40] Craig, D. P.; Thirunamachandran, R.: *Molecular quantum electrodynamics*; Academic: New York, 1984.

[41] Akins, D. L.; Akpabli, C. K.; Li, X. Surface potential dependence of enhanced Raman bands of aggregated cyanine dyes. *J. Phys. Chem.* 1989, *93*, 1977–1984.

[42] Okabayashi, H.; Yoshida, T.; Ikeda, T.; Matsuura, H.; Kitagawa, T. PO_2^- symmetric-stretching Raman line and molecular aggregation states of barium dialkyl phosphates. *J. Am. Chem. Soc.* 1982, *104*, 5399–5402.

[43] Akins L. Daniel Enhanced Raman scattering by molecular nanoaggregates. *Nanomater. Nanotechnol.* 2014, 1.

[44] Ren, B.; Tian, Z. Q.; Guo, C.; Akins, D. L. Confocal microprobe Raman spectroscopy for investigating the aggregation process at the liquid/air interface. *Chem. Phys. Lett.* 2000, *328*, 17–22.

[45] Guo, C.; Aydin, M.; Zhu, H. R.; Akins, D. L. Density functional theory used in structure determinations and Raman band assignments for pseudoisocyanine and its aggregate. *J. Phys. Chem. B* 2002, *106*, 5447–5454.

[46] Aydin, M.; Dede, O.; Akins, D. L. Density functional theory and Raman spectroscopy applied to structure and vibrational mode analysis of 1,1′,3,3′-tetraethyl-5,5′,6,6′-tetrachloro-benzimidazolocarbocyanine iodide and its aggregate. *J. Chem. Phys.* 2011, *134*.

[47] Akins, D. L.; Zhuang, Y. H.; Zhu, H. R.; Liu, J. Q. Raman excitation-spectra of exciton-phonon modes of aggregated 2,2′-cyanine using an internal Raman standard. *J. Phys. Chem.* 1994, *98*, 1068–1072.

[48] Akins, D. L.; Zhu, H. R.; Guo, C. Absorption and Raman-scattering by aggregated meso-tetrakis(p-sulfonatophenyl)porphine. *J. Phys. Chem.* 1994, *98*, 3612–3618.

[49] Akins, D. L.; Zhu, H. R.; Guo, C. Near-infrared-excited fourier-transform Raman-spectroscopic study of covalently-linked porphyrin viologen compounds. *J. Phys. Chem.* 1993, *97*, 8681–8684.

[50] Akins, D. L.; Zhu, H. R. Raman excitation-spectra of coupled intramolecular intermolecular vibronic modes of aggregated 4,4′-cyanine. *Langmuir* 1992, *8*, 546–550.

[51] Akins, D. L.; Ozcelik, S.; Zhu, H. R.; Guo, C. Aggregation-enhanced Raman scattering of a cyanine dye in homogeneous solution. *J. Phys. Chem. A* 1997, *101*, 3251–3259.

[52] Akins, D. L.; Macklin, J. W.; Parker, L. A.; Zhu, H. R. Raman excitation-spectra of aggregate modes of 2,2′-cyanine. *Chem. Phys. Lett.* 1990, *169*, 564–568.

[53] Akins, D. L.; Macklin, J. W. Dependence of Raman-scattering by aggregated 2,2′-cyanine on PH and excitation wavelength. *J. Phys. Chem.* 1989, *93*, 5999–6007.

[54] Akins, D. L.; Lombardi, J. R. Excitation wavelength dependence of enhanced Raman bands of aggregated molecules. *Chem. Phys. Lett.* 1987, *135*, 495–500.

[55] Gaufrès, E.; Tang, N. Y. W.; Lapointe, F.; Cabana, J.; Nadon, M. A.; Cottenye, N.; Raymond, F.; Szkopek, T.; Martel, R. Giant Raman scattering from J-aggregated dyes inside carbon nanotubes for multispectral imaging. *Nat. Photonics* 2013, *8*, 72–78.

[56] Kalbac, M.; Kavan, L.; Gorantla, S.; Gemming, T.; Dunsch, L. Sexithiophene encapsulated in a single-walled carbon nanotube: an in situ Raman spectroelectrochemical study of a peapod structure. *Chemistry* 2010, *16*, 11753–11759.

[57] Hasobe, T.; Fukuzumi, S.; Kamat, P. V. Ordered assembly of protonated porphyrin driven by single-wall carbon nanotubes. J- and H-aggregates to nanorods. *J. Am. Chem. Soc.* 2005, *127*, 11884–11885.

[58] Rao, A. M.; Zhou, P.; Wang, K. A.; Eklund, P. C. Photoinduced polymerization of solid C_{60} films. *Science* 1993, *259*, 952–955.

[59] Perumal, S.; Minaev, B.; Agren, H. Spin-spin and spin-orbit interactions in nanographene fragments: a quantum chemistry approach. *J. Chem. Phys.* 2012, *136*, 104702.

[60] Ferrari, A. C.; Meyer, J. C.; Scardaci, V.; Casiraghi, C.; Lazzeri, M.; Mauri, F.; Piscanec, S.; Jiang, D.; Novoselov, K. S.; Roth, S.; Geim, A. K. Raman spectrum of graphene and graphene layers. *Phys. Rev. Lett.* 2006, *97*, 187401.

[61] Graf, D.; Molitor, F.; Ensslin, K.; Stampfer, C.; Jungen, A.; Hierold, C.; Wirtz, L. Spatially resolved raman spectroscopy of single- and few-layer graphene. *Nano Lett.* 2007, *7*, 238–242.

[62] Zhou, Q.; Pang, S. F.; Wang, Y.; Ma, J. B.; Zhang, Y. H. Confocal Raman studies of the evolution of the physical state of mixed phthalic acid/ammonium sulfate aerosol droplets and the effect of substrates. *J. Phys. Chem. B* 2014, *118*, 6198–6205.

[63] Zhao, L. J.; Zeng, Q. X.; Zhang, Y. H. State of water in supersaturated nitrate aerosols disclosed by the Raman difference spectra. *J. Phys. Chem. A* 2009, *113*, 215–220.

[64] Zhao, L. J.; Wang, F.; Zhang, K.; Zeng, Q. X.; Zhang, Y. H. Deliquescence and efflorescence processes of aerosol particles studied by in situ FTIR and Raman spectroscopy. *Chin. J. Chem. Phys.* 2008, *21*, 1–11.

[65] Wang, F.; Zhang, Y. H.; Zhao, L. J.; Zhang, H.; Cheng, H.; Shou, J. J. Micro-Raman study on the conformation behavior of succinate in supersaturated sodium succinate aerosols. *Phys. Chem. Chem. Phys.* 2008, *10*, 4154–4158.

[66] Tang, M. J.; Camp, J. C. J.; Rkiouak, L.; McGregor, J.; Watson, I. M.; Cox, R. A.; Kalberer, M.; Ward, A. D.; Pope, F. D. Heterogeneous interaction of SiO_2 with N_2O_5: aerosol flow tube and single particle optical levitation-Raman spectroscopy studies. *J. Phys. Chem. A* 2014, *118*, 8817–8827.

[67] Symes, R.; Gilham, R. J. J.; Sayer, R. M.; Reid, J. P. An investigation of the factors influencing the detection sensitivity of cavity enhanced Raman scattering for probing aqueous binary aerosol droplets. *Phys. Chem. Chem. Phys.* 2005, *7*, 1414–1422.

[68] Schill, G. P.; Tolbert, M. A. Heterogeneous ice nucleation on simulated sea-spray aerosol using Raman microscopy. *J. Phys. Chem. C* 2014, *118*, 29234–29241.

[69] Gen, M.; Lenggoro, W. Probing a dip-coated layer of organic molecules by an aerosol nanoparticle sensor with sub-100 nm resolution based on surface-enhanced Raman scattering. *RSC Adv.* 2015, *5*, 5158–5163.

[70] Gaffney, J. S.; Marley, N. A.; Smith, K. J. Characterization of fine mode atmospheric aerosols by Raman microscopy and diffuse reflectance FTIR. *J. Phys. Chem. A* 2015, *119*, 4524–4532.

[71] Davies, J. F.; Wilson, K. R. Raman spectroscopy of isotopic water diffusion in ultraviscous, glassy, and gel states in aerosol by use of optical tweezers. *Anal. Chem.* 2016, *88*, 2361–2366.

[72] Craig, R. L.; Bondy, A. L.; Ault, A. P. Surface enhanced Raman spectroscopy enables observations of previously undetectable secondary organic aerosol components at the individual particle level. *Anal. Chem.* 2015, *87*, 7510–7514.

[73] Buajarern, J.; Mitchem, L.; Reid, J. P. Characterizing the formation of organic layers on the surface of inorganic/aqueous aerosols by Raman spectroscopy. *J. Phys. Chem. A* 2007, *111*, 11852–11859.

[74] Ault, A. P.; Zhao, D.; Ebben, C. J.; Tauber, M. J.; Geiger, F. M.; Prather, K. A.; Grassian, V. H. Raman microspectroscopy and vibrational sum frequency generation spectroscopy as probes of the bulk and surface compositions of size-resolved sea spray aerosol particles. *Phys. Chem. Chem. Phys.* 2013, *15*, 6206–6214.

[75] Arunagirinathan, M. A.; Roy, M.; Dua, A. K.; Manohar, C.; Bellare, J. R. Micro-Raman investigations of myelins in aerosol-OT/water system. *Langmuir* 2004, *20*, 4816–4822.

[76] Aker, P. M.; Zhang, J. X.; Nichols, W. Nitrate ion detection in aerosols using morphology-dependent stimulated Raman scattering. *J. Chem. Phys.* 1999, *110*, 2202–2207.

[77] Aggarwal, R. L.; Di Cecca, S.; Farrar, L. W.; Jeys, T. H. Chemical aerosol detection and identification using Raman scattering. *J. Raman Spectrosc.* 2014, *45*, 677–679.

[78] Batonneau, Y.; Sobanska, S.; Laureyns, J.; Bremard, C. Confocal microprobe Raman imaging of urban tropospheric aerosol particles. *Environ. Sci. Technol.* 2006, *40*, 1300–1306.

[79] An, P.; Yuan, C. Q.; Liu, X. H.; Xiao, D. B.; Luo, Z. X. Vibrational spectroscopic identification of isoprene, pinenes and their mixture. *Chin. Chem. Lett.* 2016, *27*, 527–534.

[80] King, M. D.; Thompson, K. C.; Ward, A. D. Laser tweezers Raman study of optically trapped aerosol droplets of Seawater and oleic acid reacting with ozone: implications for cloud-droplet properties. *J. Am. Chem. Soc.* 2004, *126*, 16710–16711.

[81] Buehler, M. F.; Allen, T. M.; Davis, E. J. Microparticle Raman-spectroscopy of multicomponent aerosols. *J. Colloid Interface Sci.* 1991, *146*, 79–89.

[82] Xu, G.; Fang, Y. Studies of surface-enhanced Raman scattering of C60 Langmuir–Blodgett film on a new substrate. *Spectrochim. Acta A* 2008, *70*, 104–108.

[83] Wu, L. X.; Xu, W. Q.; Qin, L. D.; Wang, C. S. Self-assembly and Langmuir-Blodgett (LB) film of a novel hydrogen-bonded complex: a surface enhanced Raman scattering (SERS) study. *Colloid Surf. A* 2002, *198-200*, 135–140.

[84] Wu, S. X.; Huang, J. G.; Li, C.; Liang, Y. Q. Fourier transform surface-enhanced Raman scattering of single-layer nucleolipid Langmuir-Blodgett films on silver island film substrates. *J. Colloid Interface Sci.* 2004, *270*, 309–314.

[85] Constantino, C. J. L.; Aroca, R. F.; Mendonca, C. R.; Mello, S. V.; Balogh, D. T.; Oliveira, O. N. Surface enhanced fluorescence and Raman imaging of Langmuir-Blodgett azopolymer films. *Spectrochim. Acta A* 2001, *57*, 281–289.

[86] Siu, G. G.; Yulong, L.; Shishen, X.; Jingmei, X.; Tiankai, L.; Linge, X. Surface-enhanced Raman spectroscopy of monolayer C_{60} Langmuir-Blodgett films. *Thin Solid Films* 1996, *274*, 147–149.

[87] Puggelli, M.; Ricceri, R.; Gabrielli, G. SERS and molecular orientation in Langmuir-Blodgett films deposited onto smooth copper surfaces. *Langmuir* 1996, *12*, 4417–4420.

[88] Urai, Y.; Itoh, K. Surface-enhanced photopolymerization of a diacetylene derivative in Langmuir-Blodgett films on a silver island film. *J. Phys. Chem. B* 1998, *102*, 3765–3772.

[89] Constantino, C. J. L.; Aroca, R. F. Surface-enhanced resonance Raman scattering imaging of Langmuir-Blodgett monolayers of bis(benzimidazo)perylene on silver island films. *J. Raman Spectrosc.* 2000, *31*, 887-890.

[90] Masuda, H.; Fukuda, K. Ordered metal nanohole arrays made by a 2-step replication of honeycomb structures of anodic alumina. *Science* 1995, *268*, 1466–1468.

[91] Masuda, H.; Asoh, H.; Watanabe, M.; Nishio, K.; Nakao, M.; Tamamura, T. Square and triangular nanohole array architectures in anodic alumina. *Adv. Mater.* 2001, *13*, 189–192.

[92] Han, F.; Meng, G.; Xu, Q.; Zhu, X.; Zhao, X.; Chen, B.; Li, X.; Yang, D.; Chu, Z.; Kong, M. Alumina-sheathed nanocables with cores consisting of various structures and materials. *Angew. Chem. Int. Ed.* 2011, *50*, 2036–2040.

[93] Luo, Z.; Liu, Y.; Kang, L.; Wang, Y.; Fu, H.; Ma, Y.; Yao, J.; Loo, B. H. Controllable nanonet assembly utilizing a pressure-difference method based on anodic aluminum oxide templates. *Angew. Chem. Int. Ed.* 2008, *47*, 8905–8908.

[94] Luo, Z.; Yang, W.; Peng, A.; Ma, Y.; Fu, H.; Yao, J. The fabrication of TiO_2 nanorods from TiO_2 nanoparticles by organic protection assisted template method. *Nanotechnology* 2009, *20*, 345601.

[95] Luo, Z.; Fang, Y. Structural influence on Raman scattering of a new C_{60} thin film prepared by AAO template with the method of pressure difference. *J. Comb. Chem.* 2006, *8*, 500–504.

[96] Luo, Z.; Fang, Y.; Zhang, P. Surface enhanced raman scattering of gold/c60 (/c70) nanoclusters deposited on AAO nano-sieve. *Vib. Spectrosc.* 2006, *41*, 37-41.

[97] Luo, Z.; Yang, W.; Peng, A.; Ma, Y.; Fu, H.; Yao, J. Net-like assembly of au nanoparticles as a highly-active substrate for surface enhanced Raman and infrared spectroscopy. *J. Phys. Chem. A* 2009, *113*, 2467–2472.

[98] Luo, Z.; Loo, B. H.; Yao, J.: Uniformly-assembled metal nanoparticles on anodic aluminum oxide (AAO) applied in surface-enhanced Raman spectroscopy. In *MRS Spring Meeting*: San Francisco, California, 2011.

[99] Luo, Z.; Zhao, Y.; Yang, W.; Peng, A.; Ma, Y.; Fu, H.; Yao, J. Core-shell nanopillars of fullerene C_{60}/C_{70} loading with colloidal Au nanoparticles:A Raman scattering investigation. *J. Phys. Chem. A* 2009, *113*, 9612–9616.

[100] Liu, J.; White, I.; DeVoe, D. L. Nanoparticle-functionalized porous polymer monolith detection elements for surface-enhanced Raman scattering. *Anal. Chem.* 2011, *83*, 2119–2124.

[101] Peters, E. C.; Svec, F.; Frechet, J. M. J. Rigid macroporous polymer monoliths. *Adv. Mater.* 1999, *11*, 1169–1181.

[102] Fu, H.; Xiao, D.; Yao, J.; Yang, G. Nanofibers of 1,3-diphenyl-2-pyrazoline induced by cetyltrimethylammonium bromide micelles. *Angew. Chem. Int. Ed.* 2003, *42*, 2883–2886.

[103] Tian, Z. Q.; Ren, B.; Li, J. F.; Yang, Z. L. Expanding generality of surface-enhanced Raman spectroscopy with borrowing SERS activity strategy. *Chem. Commun.* 2007, 3514–3534.

[104] Park, S.; Yang, P.; Corredor, P.; Weaver, M. J. Transition metal-coated nanoparticle films: vibrational characterization with surface-enhanced Raman scattering. *J. Am. Chem. Soc.* 2002, *124*, 2428–2429.

[105] Tian, Z. Q.; Ren, B. Adsorption and reaction at electrochemical interfaces as probed by surface-enhanced Raman spectroscopy. *Annu. Rev. Phys. Chem.* 2004, *55*, 197–229.

[106] Park, W. H.; Kim, Z. H. Charge transfer enhancement in the SERS of a single molecule. *Nano Lett.* 2010, *10*, 4040–4048.

[107] Chen, K.; Leona, M.; Vo-Dinh, T. Surface-enhanced Raman scattering for identification of organic pigments and dyes in works of art and cultural heritage material. *Sens. Rev.* 2007, *27*, 109–120.

[108] Chen, K.; Vo-Dinh, K. C.; Yan, F.; Wabuyele, M. B.; Vo-Dinh, T. Direct identification of alizarin and lac dye on painting fragments using surface-enhanced Raman scattering. *Anal. Chim. Acta* 2006, *569*, 234–237.

[109] Jurasekova, Z.; Domingo, C.; Garcia-Ramos, J. V.; Sanchez-Cortes, S. In situ detection of flavonoids in weld-dyed wool and silk textiles by surface-enhanced Raman scattering. *J. Raman Spectrosc.* 2008, *39*, 1309–1312.

[110] Brosseau, C. L.; Gambardella, A.; Casadio, F.; Van Duyne R. P.; Grzywacz, C. M.; Wouters, J. Ad-hoc surface-enhanced Raman spectroscopy methodologies for the detection of artist dyestuffs: thin layer chromatography-surface enhanced raman spectroscopy and in situ on the fiber analysis. *Anal. Chem.* 2009, *81*, 3056–3062.

[111] Wustholz, K. L.; Brosseau, C. L.; Casadio, F.; Van Duyne, R. P. Surface-enhanced Raman spectroscopy of dyes: from single molecules to the artists' canvas. *Phys. Chem. Chem. Phys.* 2009, *11*, 7350–7359.

[112] Luo, Z.; Smith, J. C.; Goff, T. M.; Adair, J. H.; Castleman, A. W., Jr. Gold cluster coatings enhancing Raman scattering from surfaces: ink analysis and document identification. *Chem. Phys.* 2013, *423*, 73–75.

[113] Anema, J. R.; Li, J. F.; Yang, Z. L.; Ren, B.; Tian, Z. Q.: Shell-isolated nanoparticle-enhanced raman spectroscopy: expanding the versatility of surface-enhanced Raman scattering. In *Annu. Rev. Anal. Chem.*; Cooks, R. G., Yeung, E. S., Eds.; Annual Review of Analytical Chemistry; Annual Reviews: Palo Alto, 2011; Vol. 4; pp. 129–150.

[114] Li, J. F.; Huang, Y. F.; Ding, Y.; Yang, Z. L.; Li, S. B.; Zhou, X. S.; Fan, F. R.; Zhang, W.; Zhou, Z. Y.; Wu, D. Y.; Ren, B.; Wang, Z. L.; Tian, Z. Q. Shell-isolated nanoparticle-enhanced Raman spectroscopy. *Nature* 2010, *464*, 392–395.

[115] Moskovits, M. Surface-enhanced spectroscopy. *Rev. Mod. Phys.* 1985, *57*, 783–826.

[116] Kneipp, K.; Moskovits, M.; Kneipp, H.: *Surface-enhanced Raman scattering: physics and applications*; Springer: Berlin & New York, 2006; Vol. 103.

[117] Wu, D. Y.; Li, J. F.; Ren, B.; Tian, Z. Q. Electrochemical surface-enhanced Raman spectroscopy of nanostructures. *Chem. Soc. Rev.* 2008, *37*, 1025–1041.

[118] Luo, Z.; Fang, Y. Progress in application of surface enhanced Raman scattering spectrum technique. *Spectrosc. Spectral Anal.* 2006, *26*, 358–364.

[119] Wuelfert, S.; Herren, D.; Leutwyler, S. Reply to "The intramolecular fundamentals of the water dimer". *J. Chem. Phys.* 1988, *88*, 52–56.

[120] Wuelfert, S.; Herren, D.; Leutwyler, S. Supersonic jet CARS spectra of small water clusters. *J. Chem. Phys.* 1987, *86*, 3751.

[121] Nelander, B. The intramolecular fundamentals of the water dimer. *J. Chem. Phys.* 1988, *88*, 5254.

[122] Otto, K. E.; Xue, Z.; Zielke, P.; Suhm, M. A. The Raman spectrum of isolated water clusters. *Phys. Chem. Chem. Phys.* 2014, *16*, 9849–9858.

[123] Farrag, M.; Tschurl, M.; Dass, A.; Heiz, U. Infra-red spectroscopy of size selected Au25, Au38 and Au144 ligand protected gold clusters. *Phys. Chem. Chem. Phys.* 2013, *15*, 12539–12542.

[124] Petroski, J.; Chou, M.; Creutz, C. The coordination chemistry of gold surfaces: formation and far-infrared spectra of alkanethiolate-capped gold nanoparticles. *J. Organomet. Chem.* 2009, *694*, 1138–1143.

[125] Levin, C. S.; Janesko, B. G.; Bardhan, R.; Scuseria, G. E.; Hartgerink, J. D.; Halas, N. J. Chain-length-dependent vibrational resonances in alkanethiol self-assembled monolayers observed on plasmonic nanoparticle substrates. *Nano Lett.* 2006, *6*, 2617–2621.

[126] Burgi, T. Properties of the gold-sulphur interface: from self-assembled monolayers to clusters. *Nanoscale* 2015, *7*, 15553–15567.

[127] Varnholt, B.; Oulevey, P.; Luber, S.; Kumara, C.; Dass, A.; Bürgi, T. Structural information on the Au–S interface of thiolate-protected gold clusters: a Raman spectroscopy study. *J. Phys. Chem. C* 2014, *118*, 9604–9611.

[128] Yasuike, T.; Nobusada, K. Raman enhancement by plasmonic excitation of structurally-characterized metal clusters: Au8, Ag8, and Cu8. *Phys. Chem. Chem. Phys.* 2013, *15*, 5424–5429.

[129] Tomas, M.; Tinti, A.; Bofill, R.; Capdevila, M.; Atrian, S.; Torreggiani, A. Comparative Raman study of four plant metallothionein isoforms: insights into their Zn(II) clusters and protein conformations. *J. Inorg. Biochem.* 2016, *156*, 55–63.

[130] Su, J. P.; Lee, Y. T.; Lu, S. Y.; Lin, J. S. Chemical mechanism of surface-enhanced Raman scattering spectrum of pyridine adsorbed on Ag cluster: ab initio molecular dynamics approach. *J. Comput. Chem.* 2013, *34*, 2806–2815.

[131] Siebert, E.; Rippers, Y.; Frielingsdorf, S.; Fritsch, J.; Schmidt, A.; Kalms, J.; Katz, S.; Lenz, O.; Scheerer, P.; Paasche, L.; Pelmenschikov, V.; Kuhlmann, U.; Mroginski, M. A.; Zebger, I.; Hildebrandt, P. Resonance Raman spectroscopic analysis of the [NiFe] active site and the proximal [4Fe-3S] cluster of an O_2-tolerant membrane-bound hydrogenase in the crystalline state. *J. Phys. Chem. B* 2015, *119*, 13785–13796.

[132] Schmidt, M.; Fernandez, J. M.; Faruk, N.; Nooijen, M.; Le Roy, R. J.; Morilla, J. H.; Tejeda, G.; Montero, S.; Roy, P. N. Raman vibrational shifts of small clusters of hydrogen isotopologues. *J. Phys. Chem. A* 2015, *119*, 12551–12561.

[133] Santos, J. J.; Ando, R. A.; Toma, S. H.; Corio, P.; Araki, K.; Toma, H. E. Surface enhanced Raman spectroelectrochemistry of a mu-oxo triruthenium acetate cluster: an experimental and theoretical approach. *Inorg. Chem.* 2015, *54*, 9656–9663.

[134] Rudolph, W. W.; Fischer, D.; Tomney, M. R.; Pye, C. C. Indium(III) hydration in aqueous solutions of perchlorate, nitrate and sulfate. Raman and infrared spectroscopic studies and ab-initio molecular orbital calculations of indium(III)-water clusters. *Phys. Chem. Chem. Phys.* 2004, *6*, 5145–5155.

[135] Pradhani, A.; Halder, O.; Nozaki, S.; Rath, S. Raman modes, dipole moment and chirality in periodically positioned Au8clusters. *RSC Adv.* 2015, *5*, 65208–65213.

[136] Faruk, N.; Schmidt, M.; Li, H.; Le Roy, R. J.; Roy, P. N. First-principles prediction of the Raman shifts in parahydrogen clusters. *J. Chem. Phys.* 2014, *141*, 014310.

[137] Chen, L.; Gao, Y.; Cheng, Y.; Su, Y.; Wang, Z.; Li, Z.; Zhang, R. Q. Strong core@shell dependence in surface-enhanced Raman scattering of pyridine on stable 13-atom silver-caged bimetallic clusters. *J. Phys. Chem. C* 2015, *119*, 17429–17437.

[138] Chen, J.; Zhang, H.; Liu, X.; Yuan, C.; Jia, M.; Luo, Z.; Yao, J. Charge-transfer interactions between TCNQ and silver clusters Ag_{20} and Ag_{13}. *Phys. Chem. Chem. Phys.* 2016, *18*, 7190–7196.

[139] Luo, Z.; Reber, A. C.; Jia, M.; Blades, W. H.; Khanna, S. N.; Castleman, A. W. What determines if a ligand activates or passivates a superatom cluster? *Chem. Sci.* 2016, *7*, 3067–3074.

[140] Chen, J.; Luo, Z.; Yao, J. Theoretical study of tetrahydrofuran-stabilized Al_{13} superatom cluster. *J. Phys. Chem. A* 2016, *120*, 3950–3957.

IntechOpen